Received: 2 August 2018 | Revised: 19 October 2018 | Accepted: 20 November 2018

DOI: 10.4218/etrij.2018-0420

SPECIAL ISSUE

WILEY ETRI Journal

Off-axis self-reference digital holography in the visible and far-infrared region

Vittorio Bianco | **Melania Paturzo** | **Andrea Finizio** | **Pietro Ferraro**

Institute of Applied Sciences and Intelligent Systems, Italian National Research Council (ISASI-CNR), Pozzuoli (Napoli), Italy.

Correspondence
Vittorio Bianco, Institute of Applied Sciences and Intelligent Systems, Italian National Research Council (ISASI-CNR), Pozzuoli (Napoli), Italy.
Email: v.bianco@isasi.cnr.it

Funding information
This research was supported by the project "Databenc REMIAM, REte dei Musei Intelligenti and Avanzata Multimedialità."

Recent advances in digital holography in the far-infrared region of the spectrum have demonstrated the potential use of digital holography in homeland security as a tool to observe hostile environments in which smoke, flames, and dust impair vision. However, to make this application practical, it is necessary to simplify the optical setup. Here, we show an off-axis, self-reference scheme that spills the reference beam out from the object beam itself and avoids the need for a complex interferometric arrangement. We demonstrate that this scheme allows the reconstruction of high-quality holograms of objects captured under visible as well as far-infrared light exposure. This could pave the way to the industrialization of holographic systems to enable users to see through fire. Moreover, the quantitative nature of the holographic signal is preserved. Thus, the reported results demonstrate the possibility to use this setup for optical metrology.

KEYWORDS
digital holography, 3D imaging, interferometry, optical metrology, infrared imaging, flames, security

1 | INTRODUCTION

Long-wavelength infrared radiation (LWIR) digital holography (DH) shows some advantages when it is compared to the equivalent technique in visible light, which makes it more advisable for nondestructive testing and other applications in the field of aerospace [1–5], cultural heritage [6,7], or security [8,9].

Indeed, the use of long infrared (IR) wavelengths reduces the sensitivity of interferometric measurements to vibrations and seismic noise by approximately 20 times with respect to DH in the visible range. In turn, the measurement range increases by the same factor, which corresponds to the ratio between the IR and visible wavelengths. Moreover, the high power of CO_2 laser sources, emitting lines around 9.5 μm and 10.6 μm, and the possibility to have a large field of view make the extension of holographic/speckle techniques to LWIR especially advantageous for industrial applications [10–12]. In fact, the minimum distance, $z_{0,\min}$, between the object and the detector, whose value can be calculated as $z_{0,\min} = (d_p D)/\lambda$ is inversely proportional to the used wavelength λ and directly proportional to the camera pixel pitch, d_p, and the object linear dimension, D [13]. From another point of view, the linear dimension of the objects that can be imaged by LWIR-DH increases with the wavelength, and one can take advantage of the wavelength augment when passing from visible to IR sources. The opportunity of recording digital holograms of meter-size objects paves the way to the use of LWIR-DH in the field of cultural heritage, for example, for 3D imaging and display of goods of cultural interest, such as statuettes and sculptures made of various materials, exploitable for academic purposes and as added-value products in next-generation virtual museums. The holograms acquired by LWIR-DH can be optically reconstructed using a visible laser and a spatial light modulator (SLM) to achieve this purpose. Moreover, by means of a numerical procedure, synthetic scenes can be created and optically displayed [6,7].

Remarkably, LWIR-DH finds applications in the security field as well, where it can be used to see through smoke and flames [8], being, in principle, suitable for exploring fire scenes during search and rescue operations, or in industrial sites, where furnaces and boiler equipment can be monitored in real time to prevent quality problems during the entire process line. One of the reasons for the success of LWIR-DH is the lensless setup, which avoids the saturation of the IR sensor elements by unfocused and noncoherent flame emission [8]. However, the complexity of the bulky interferometric setup makes the imaging apparatus unportable, but portability is a necessary condition for on-field applications. To overcome this issue, Bianco and others proposed a lens-based noninterferometric setup based on laser raster scanning and matched bandpass filtering to obtain a portable compact system for real-time inspection of the fire scene [9]. Nevertheless, the simplicity and portability of the proposed system was paid for by a poorer signal-to-noise ratio (SNR) due to the flame radiation emitted in the filter passband.

The optimal configuration to tackle the problem should be a simplified holographic setup, avoiding the two-arm arrangement. Therefore, in this paper, we propose an off-axis self-reference setup to combine the advantages of the interferometric system with the portability feature. Here, we demonstrate for the first time that such a holographic setup works properly for LWIR.

2 | EXPERIMENTAL METHOD

We implement an experimental setup based on a wavefront division configuration [14]. The idea is to use part of the object beam to obtain a reference beam by inserting a pinhole in the optical path. This has the effect of cleaning the wavefront from the object modulation, so that a reference wavefront can be spilled out. Thus, we obtain a simple self-reference setup in an off-axis configuration both for the visible and IR laser sources, as shown in Figure 1A, B, respectively.

In the visible setup, the light source (Mod. Torus by Laser Quantum, wavelength = 532 nm, power = 500 mW) impinges on the object mounted on a motorized stage and equipped with two-axis piezo-tilters. Part of the scattered light is collected by a lens (Doublet F = 50 mm, diameter = 50 mm) that focuses the light on a pinhole, 100 μm^2 in size, obtained by using a two-axis variable slit. It acts as a spatial filter, effectively creating a reference beam by erasing the sample information, as shown in the inset of Figure 1A. In this way, a very low intensity of the reference beam results. Then, a mirror redirects the reference wave on a beam splitter (split ratio, R:T = 90:10), which recombines the two beams and strongly attenuates the object beam, allowing to obtain a useful object/reference beams ratio. Further improvements of the fringe visibility are achieved by introducing proper NDF filters in the object beam and by adding a polarizer just before the CCD (CMOS Camera UI-1242LE-M, IDS Imaging Systems, 1,280 × 1,024 pixels, pixel size = 5.30 μm, frame rate = 25.8 fps), used to acquire the interference patterns.

The IR setup (Figure 1B) is conceptually the same as that of the visible setup, although in this case the mirror is inserted in the object beam path with the aim to optimize the fringe visibility. In fact, the laser source (Universal Laser Systems Mod. URL-50, Wavelength = 10.6 μm, Power = 50 W) illuminates the object, positioned in front of the CCD (MicroCAM™2 Thermal Camera, Thermoteknix Systems Ltd., 640 × 480 pixels, pixel size = 17 μm, frame rate = 25 fps). Part of the light scattered by the object is collected by a mirror (gold sputtered on a glass substrate, diameter = 60 mm) that redirects this object beam on the beam recombiner, that, in turn, reflects it onto the CCD. A lens (ZnSe, f = 50 mm, diameter = 32 mm), placed in the front of the CCD, collects the other part of the object scattered light and focuses it on the pinhole, composed by the two-axis adjustable slit. The obtained divergent reference beam reaches the sensor passing through a zinc-selenide window (diameter = 40 mm, transmittance 70%, reflectance 5%), that acts as a beam recombiner, which strongly attenuates the object beam, allowing the system to obtain a useful object/reference beam ratio without adding further optical components. The distance between the object and the detector is approximately 80 cm.

Recently, Prof. Skaked's group developed an off-axis self-reference interferometer, working in the visible spectrum, by inserting a pinhole in the arm of a Mickelson interferometer [15]. However, the configuration proposed in [15] corresponds to an intensity division configuration, whereas the scheme we propose can be thought as a wavefront division setup. Moreover, the technique proposed in [15] requires specialized optical elements for the creation of reference wavefront, whereas in this work, we use a portion of the object beam to create the reference one by means of few optical elements, making compact geometries possible.

Moreover, similar self-reference DH techniques have been proposed based on wavefront division, by using two lenses [16] or in lensless configuration [17]. However, both papers deal with a DH setup in transmission mode, working only for transparent samples. In contrast, our technique concerns opaque objects, in reflection configuration, and we demonstrate it is suitable both in visible and in far-IR region.

Using the setups shown in Figure 1, we carried out experiments to assess the ability of the proposed self-reference

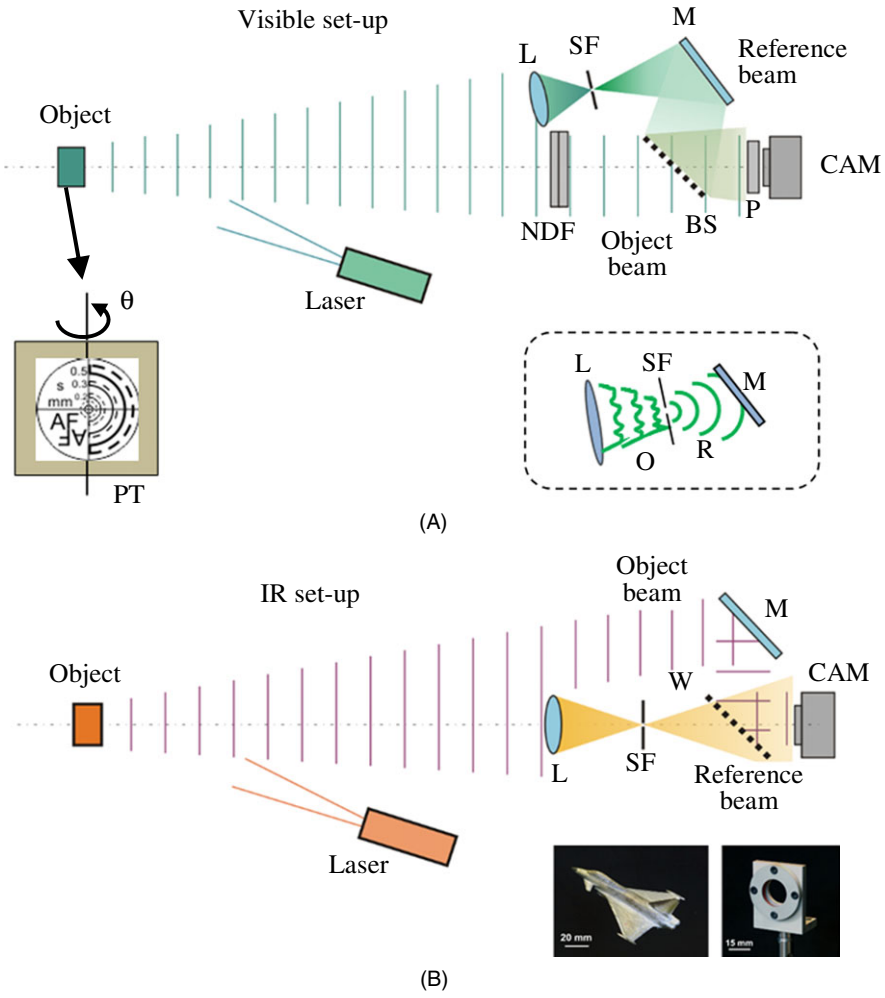

FIGURE 1 Self-reference scheme. Sketch of the experimental setup in the case of (A) visible light and (B) LWIR light. PT, piezo-tilter; BS, beam splitter; L, lens; O, object beam; R, reference beam; M, mirror; P, polarizer; SF, spatial filter; NDF, neutral-density filter; W, window. In the inset of (A), the optical filtering effect of the slits is sketched; a reference beam is generated by cleaning the wavefront from the object modulation. Photos of the objects used in experimental tests are shown in the insets of (A) and (B)

scheme to provide holograms that yield all the useful capabilities of a conventionally acquired DH. In order to demonstrate the effectiveness of the self-reference scheme, we acquired holograms in lensless reflection mode of different diffusive objects probed by visible as well as far-IR coherent light. The acquired holograms are numerically propagated along the optical axis, and the best-focus plane is found by optimizing the sharpness of the amplitude reconstructions at different propagation distances. Besides flexible refocusing and imaging using different wavelengths of the probing coherent beams, the quantitative nature of DH imaging has to be maintained with the introduced scheme to propose the setups in Figure 1 as a valuable tool for optical metrology.

3 | EXPERIMENTAL RESULTS

In this section, we provide the results of experiments carried out with the aim to assess both the capabilities of the introduced scheme as an imaging tool for visible and IR coherent light, and the assessment of the system as a quantitative tool for optical metrology through the use of phase images.

3.1 | Amplitude reconstruction

In the first experiment, we imaged a test target, shown on the left of Figure 1A, through the self-reference setup using visible wavelength $\lambda_{vis} = 532$ nm. The object was placed on a tilter connected to a piezoelectric actuator driven by a known external voltage, P_V. Initially, we set $P_V = 0$ V, so that no mechanical rotation was delivered to the object. Figure 2 shows two examples of lensless holograms, H, captured in this condition. In particular, Figure 2A shows the DH, and Figure 2B shows the detail of the area in the green box of Figure 2A. The hologram does not show a formed image of the object, as expected due to the lensless setup. By inspection of Figure 2A, it is apparent instead the formation of two distinct sets of speckle patterns. One of them is made of small and numerous speckle grains that are typical of any imaging system relying on coherent light. The size of the speckle grains depends on both geometrical factors related to the acquisition distances and the wavelength of the light source employed [18]. This must be treated as a source of noise, which can be tackled by applying denoising methods before reconstructing the hologram, or after as post-processing filters [19]. Besides, a

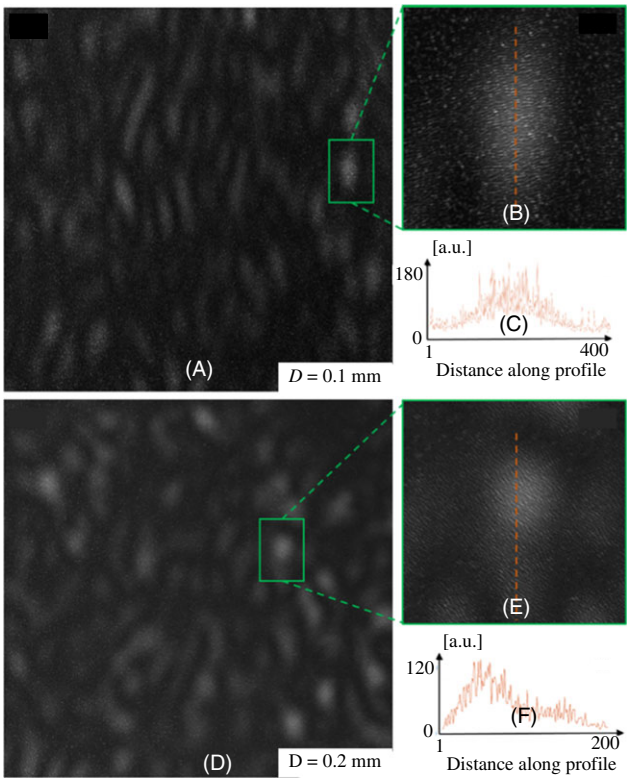

FIGURE 2 Holograms recorded under visible wavelength. (A,D) Digital holograms showing two sets of speckles. (B,E) Details of the areas in the green boxes in (A) and (D). (C,F) Cross-sectional amplitude profiles corresponding to the red dashed lines in (B) and (E). (A–C) $D = 0.1$ mm. (D–F) $D = 0.2$ mm

different set of larger grains is visible in Figure 2A, which looks like a succession of darker and brighter areas remarkably extended in size. These arise as a consequence of the presence of the lens and of the pinhole in the reference branch of the self-reference schemes in Figure 1. Optical filtering has the effect of cleaning the wavefront from the object modulation (as sketched in Figure 1A), thus generating a reference beam. However, the dimension of the pinhole ($A = 100 \times 100\ \mu m^2$) on which this beam impinges allows some of these large subjective speckles to pass through it. Thus, the fringe visibility is amplified satisfactorily in the regions where the grain is higher in amplitude and, vice versa, is poor in the dark regions of the hologram. The use of a smaller pinhole would generate a more uniform but less intense reference wave; for this reason, we cannot reduce the pinhole dimension while maintaining a good intensity ratio between reference and object beams and, consequently, a good average fringe contrast in the hologram. On the other hand, a smaller pinhole could be used with a more intense laser source or a more sensitive camera, namely, by means of more expensive setup components in respect to those used in our experimental system. The enlarged detail in Figure 2B shows one of the bright grains, and the cross-section profile shown in Figure 2C shows the amplification of the fringe signal across the red dashed line in Figure 2B. Although the fringe visibility in the dark areas is not ideal, the information content of the bright areas is enough to reconstruct a formed image of the object. This is a somehow expected result since in DH is always possible to obtain a lower resolution version of the object by using only a portion of the recorded hologram. Figures 2D–F shows another example of the visible lensless hologram captured by doubling the SF size ($D = 0.2$ mm instead of $D = 0.1$ mm). It is apparent that, having fixed the split ratio to R:T = 90:10 and the optical density of the NDF, the hologram in Figure 2D does not correspond to the optimal recording condition (too much light passes through the SF), so that the resulting fringe visibility is worse in Figure 2F than in Figure 2C. In order to use this larger SF, the split ratio or the NDF should be changed accordingly. Hence, in our experiments we kept the SF size to $D = 0.1$ mm.

Amplitude reconstructions of the circular target reported in Figure 1A are shown in Figure 3A, where the different images correspond to various propagation distances, that is, they are obtained through the propagation Fresnel functional, $F_R\{\ldots;z\}$, by setting different values of the parameter z [20]. We performed back-propagation to distances ranging from $z = 0$ cm to $z = -30$ cm. As a contrast metric, for each propagation distance, we measured the Tamura coefficient, T_C, over an area containing the first order of diffraction. When DH in reflection mode is performed, this metrics is a useful automatic focusing indicator as it is known to maximize in the object best-focus plane [21,22]. In other words, we estimate the correct propagation distance as

$$\hat{z}_F = \text{argmax}_z T_C\{|C(x,y;z)|\} \quad (1)$$

where $C(\ldots;z) = F_R\{H^{(+1)};z\}$ is the reconstruction of the first diffraction order, $H^{(+1)}$, and $T_C = \sqrt{\sigma/\mu}$ is defined as the square root of the ratio between the standard deviation and the mean value of the gray level distribution of the image in the region of interest. The Tamura coefficient is plotted in Figure 3B as a function of the propagation distance. The amplitude reconstructions shown in Figure 3A correspond to the values of T_C indicated by colored points on the plot in (B). From Figure 3, it is apparent that the sharper the image becomes, the higher T_C is. Moreover, the estimated value $\hat{z}_F$ corresponds to an image showing the object in sharp focus (see the third image in Figure 3A). This demonstrates the automatic focusing capability of holograms recorded using the self-reference scheme. Then, we captured holograms using far-IR wavelength as a coherent probing beam. At this scope, we adopted the setup sketched in Figure 1B to image two centimeter-sized objects with different reflection properties. The former was a lens holder containing some highly IR-reflective parts and the latter was a highly diffusing metal toy plane. Two

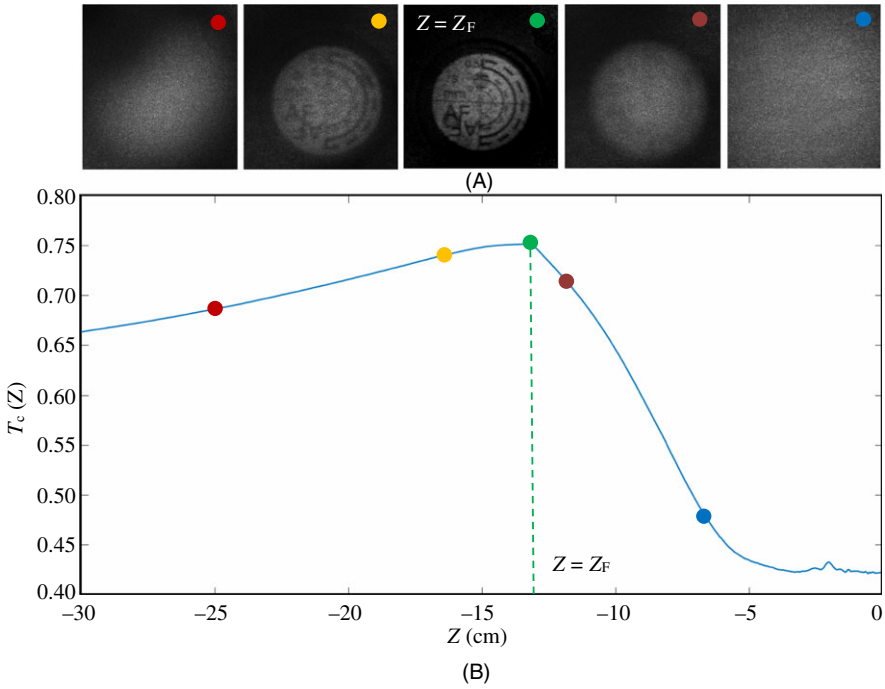

FIGURE 3 Automatic DH focusing based on contrast optimization. (A) Amplitude DH reconstructions of the test target in Figure 1(A) after propagation at various distances. (B) Tamura coefficient, T_C (z), vs. Z

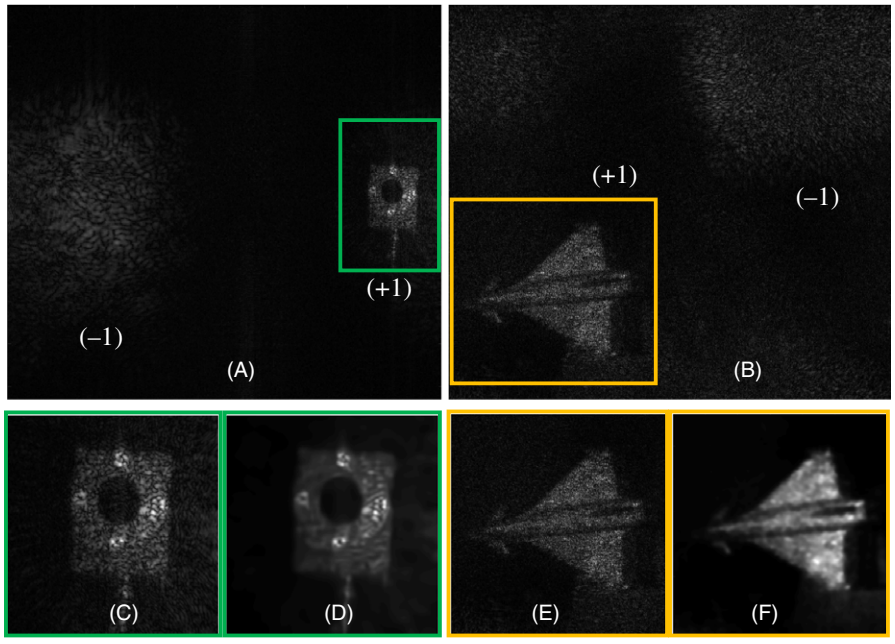

FIGURE 4 Amplitude reconstructions of digital holograms in the infrared region. (A,B) Refocused amplitude IRDH reconstructions of the objects in the photos of Figure 1(C). (C,E) Details of the first order of diffraction respectively extracted from (A) and (B). (D,F) Denoised refocused objects obtained from (C) and (E), respectively

images of the test objects are shown in the insets of Figure 1B). Due to the longer wavelength and the hardware features, the quality of DHs captured in the IR range is generally worse in terms of resolution and SNR [18].

Figure 4 shows the amplitude reconstructions of the objects. In particular, Figures 4A, B show the amplitude reconstructions of the IRDHs in the respective best-focus planes before removing the twin image. Due to the off-axis carrier, these are in principle separable from the real images by spatial filtering in a proper domain (such as in the Fourier domain). As shown in Figure 4, in this case, a partial overlapping exists between the real image in sharp focus and the spread signal representing the largely out-of-focus twin image, and acts on the reconstruction as an additional noise source. This issue can be solved by either spatially filtering the twin image in a proper domain before propagating the hologram (by propagating $H^{(+1)}$ instead of H), or directly post-processing the portion of reconstruction containing the first order of diffraction (marked as (+1) in Figures 4A, B). In this case, we followed the second route to show the capability to denoise efficiently the reconstructed object in the worst condition. Enlarged details of

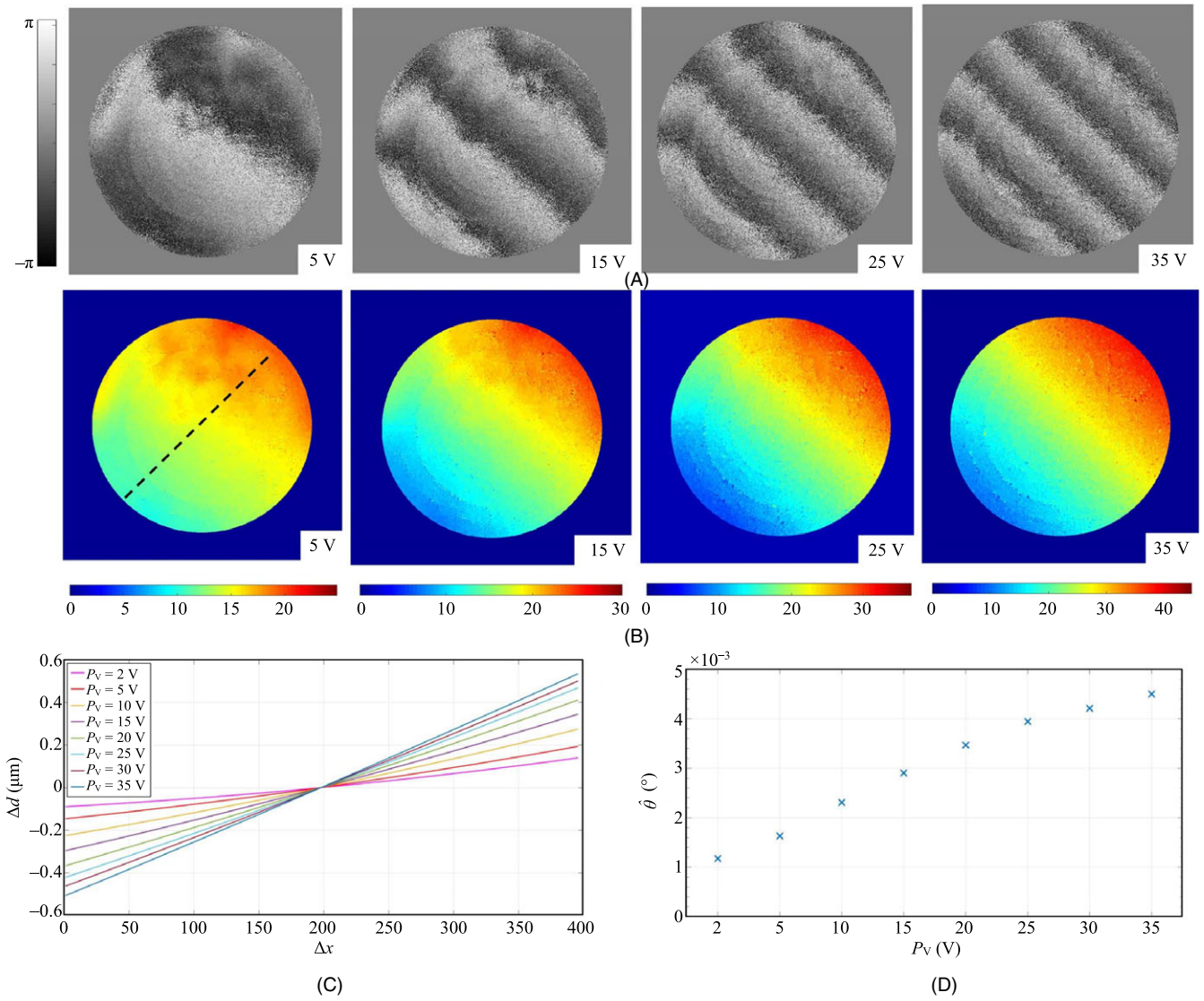

FIGURE 5 Quantitative phase imaging using through the self-reference scheme. (A) Wrapped phase maps of the test target after applying a mechanical rotation driven by a known input voltage, P_V, increasing from the left to the right. (B) Unwrapped phase maps. (C) Displacement, Δd (μm), of the target points with respect to the center of rotation. The displacement is calculated along the black dashed line shown in the leftmost figure in (B). (D) Estimated tilt angle $\hat{\theta}$ vs. P_V

the (+1) order in focus for the two objects are shown in Figures 4C and E. Although both the figures show a formed in focus image of the objects, this is severely corrupted by noise, and the lower resolution of IRDH with respect to the visible wavelength counterpart contributes to worsen the image appearance. Hence, denoising steps are required for these reconstructions. We processed the IRDH as described in [18,19,23] using the numerical multi-look 3D block-matching algorithm (MLDH-BM3D). From a single data capture, multiple holograms are obtained with numerically simulated noise diversity. This is accomplished by random resampling masks applied to the captured IRDH [23]. Then, the multiple reconstructions obtained are incoherently averaged and post-processed using the BM3D algorithm. The denoised object amplitudes are shown in Figures 4D, F, where the improvement over the corresponding images shown in (C) and (E) is remarkable. The object looks sharper and its contrast over the background is largely enhanced. This is a desired effect of the numerical ML preprocessing, which is able to reduce the relative contribution of diffuse halos in the background. Thus, the twin image is treated denoising algorithm as a noise component and reduced. The post-processing filter further augments the sharpness of the object edges and smooths the background areas while preserving the finest object details. As a result of contrast enhancement, the image appears brighter and sharper. Furthermore, its SNR augments as a processing result. The results of these experiments clearly show that it is possible to obtain IRDH reconstructions with acceptable visual quality using the simple self-reference

setup of Figure 1. We believe this will be an essential step toward the development of active IRDH imaging systems to be used on the field to see moving human size targets through smoke, dust and flames during search and rescue operations.

3.2 | Quantitative phase imaging

In order to assess whether the scheme in Figure 1 is able to yield quantitative phase maps to be used for optical metrology applications, we carried out a last experiment using probing light in the visible range. In particular, the circular target was placed on a kinematic mirror mounts (Thorlabs, KC1-PZ) equipped with NEC AE0505D08F piezoelectric stacks. We applied a known voltage $P_V \neq 0$ as an input driving signal to a piezoelectric actuator connected to the stage (referred to as PT in the sketch of Figure 1A). This has the effect of transferring a mechanical rotation to the stage of an angle $\theta \neq 0$. The holographic imaging system is sensitive to the phase of the wavefront scattered from the object. In turn, the object tilt we introduce is in principle measurable. We acquired a set of holograms of the object obtained while changing the piezo-voltage, which assumes the set of values $P_V = \{2, 5, 10, 15, 20, 25, 30, 35\}$ (V). We reconstructed the holograms and extracted the phase-contrast signal that carries information about the tilt. Figure 5 shows the results of the experiment.

In Figure 5A, we show the modulus 2π, or wrapped phase, which was obtained in correspondence of significant values of P_V. The orientation of the fringes clearly shows the tilt direction and their density gives a qualitative indication of its increment as P_V increases. The corresponding phase maps, $\psi(P_V)$, obtained after phase unwrapping [24] are shown in Figure 5B. From each of the obtained maps, we extracted the cross-sectional profile corresponding to the segment marked with a black dashed line in the left-most map of Figure 5B. The corresponding displacement, $\Delta d(\mu\text{m})$, of the target points with respect to the center of rotation (the center of the target) is obtainable as $\Delta d = (\Delta\psi P_V\lambda)/(4\pi)$ and is plotted in Figure 5C. The displacement values we measured are in good agreement with the technical specification sheet of the piezo-actuator [25]. Similarly, from the displacement, we estimated the tilt angle as a function of the driving voltage, $\hat{\theta}(P_V)^\circ$, whose plot is shown in Figure 5D. The quantitative assessment of the induced object tilt is further proof of the effectiveness of the self-reference setup in maintaining all the advantageous capabilities of DH in reflection geometry with a remarkably simplified scheme, applicable as an optical metrology tool for nondestructive testing (NDT) [26,27]. Phase recovery from LWIR holograms can be obtained with the same numerical procedure. Here, we focused on visible light holograms since the NDT based on a visible laser source is widely used in industrial applications [28–30]. Similar to standard shearography, the proposed setup has the advantages of being compact, portable, and tolerant to vibrations. Shearography in the visible range is effectively assessed for industrial needs and a recognized standard exists (ASTM E2581-14). However, unlike shearography that measures the spatial derivative of the phase, DH can retrieve the phase directly. In this sense, we believe self-reference DH can become a useful tool and find the same field of applications as visible light shearography.

4 | CONCLUSIONS

We introduced a self-reference scheme for recording DHs that avoids the need for a complex interferometric geometry. The reference beam is spilled out from the object beam itself due to the action of a double slit that cleans the wavefront from the object modulation. Thus, simple geometries to capture holograms become practicable and the holographic setup has the potential to be brought out of the laboratory. Of particular interest is the proof that was provide for the LWIR-DH case, demonstrating the possibility to obtain good quality holograms in the IR region of the spectrum. We believe this configuration applied to LWIR will enable a long step toward the industrial implementation of enhanced vision systems based on IRDH technology, such as tools to enable clear vision through fire, smoke and dust. On the other hand, we have shown that the proposed configuration maintains the quantitative feature of DH, and thus it is applicable as an optical metrology tool for NDT.

ACKNOWLEDGMENTS

We thank Antonio D'Orazio for the support in the extensive search and organization of the references.

ORCID

Vittorio Bianco https://orcid.org/0000-0003-1956-4976

REFERENCES

1. J.-F. Vandenrijt et al., *Digital holographic interferometry in the long-wave infrared and temporal phase unwrapping for measuring large deformations and rigid body motions of segmented space detector in cryogenic test*, Opt. Eng. **55** (2016), no. 12, 121723:1–121723:11.
2. M.P. Georges et al., An overview of interferometric metrology and NDT techniques and applications for the aerospace industry,

Proc. SPIE - The Int. Soc. Opt. Eng., San Diego, CA, USA, 2016, pp. 996007:1–996007:12.
3. J.-F. Vandenrijt et al., Long-wave infrared digital holography for the qualification of large space reflectors, *ICSO, Int. Conf. Pace Opt.*, Ajaccio, France, Oct. 9–12, 2012, pp. 1056403:1–1056403:5.
4. M. Georges et al., Digital holographic interferometry and ESPI at long infrared wavelengths with CO2 lasers, *Digital Holography Three-Dimensional Imaging*, Miami, FL, USA, Apr. 28–May 2, 2012, Article no. DW4C.1.
5. M.P. Georges et al., *Digital holographic interferometry with CO2 lasers and diffuse illumination applied to large space reflector metrology [Invited]*, Appl. Opt. **52** (2013), A102–A116.
6. E. Stoykova et al., *Visible reconstruction by a circular holographic display from digital holograms recorded under infrared illumination*, Opt. Lett. **37** (2012), 3120–3122.
7. M. Paturzo et al., Infrared digital holography applications for virtual museums and diagnostics of cultural heritage, *SPIE Opt. Metrology*, Munich, Germany, 2011, pp. 80840K:1–80840K:6, https://doi.org/10.1117/12.890039.
8. M. Locatelli et al., *Imaging live humans through smoke and flames using far-infrared digital holography*, Opt. Express **21** (2013), 5379–5390.
9. V. Bianco et al., *Portable IR laser system for real-time display of alive people in fire scenes*, J. Display Technol. **11** (2015), 834–838.
10. M. P. Georges et al., Speckle interferometry at 10 μm with CO2 lasers and microbolometers array, *Photonics North*, June 6–8, 2012, pp. 84121O:1–84121O:8, doi: 10.1117/12.2001440.
11. P. Poggi et al., *Remote monitoring of building oscillation modes by means of real-time Mid Infrared Digital Holography*, Sci. Rep. **6** (2016), Article no. 23688.
12. P. Mensah et al., *Scanning digital holography at 10.6 μm for large scene reconstruction*, J. Phys. Comm. **2** (2018), no. 5, Article no. 055018.
13. M. Paturzo et al., *Optical reconstruction of digital holograms recorded at 10.6 μm: Route for 3D imaging at long infrared wavelengths*, Opt. Lett. **35** (2010), 2112–2114.
14. M. Totzeck, *Interferometry, Springer Handbook of Lasers and Optics*, Springer Berlin Heidelberg, Berlin, Heidelberg, 2012. https://doi.org/10.1007/978-3-642-19409-2_16.
15. A. Nativ and N. T. Shaked, *Compact interferometric module for full-field interferometric phase microscopy with low spatial coherence illumination*, Opt. Lett. **42** (2017), 1492–1495.
16. N. Patel et al., *Wavefront division digital holographic microscopy*, Biomed. Opt. Express **9** (2018), 2779–2784.
17. W. Zhang et al., *Wavefront division digital holography*, AIP Adv. **8** (2018), Article no. 055304.
18. V. Bianco et al., *On-speckle suppression in IR digital holography*, Opt. Lett. **41** (2016), no. 22, 5226–5229.
19. V. Bianco et al., *Strategies for reducing speckle noise in digital holography*, Light Sci. Appl. **7** (2018), 48. https://doi.org/10.1038/s41377-018-0050-9.
20. P. Memmolo et al., *Numerical manipulation of digital holograms for 3D imaging and display: An overview*, Proc. IEEE **105** (2017), 892–905.
21. F. Dubois et al., *Focus plane detection criteria in digital holography microscopy by amplitude analysis*, Opt. Express **14** (2006), 5895–5908.
22. P. Memmolo et al., *Automatic focusing in digital holography and its application to stretched holograms*, Opt. Lett. **36** (2011), 1945–1947.
23. V. Bianco et al., *Random resampling masks: A non-Bayesian one-shot strategy for noise reduction in digital holography*, Opt. Lett. **38** (2013), no. 5, 619–621.
24. J. M. Bioucas-Dias and G. Valadão, *Phase unwrapping via graph cuts*, IEEE Trans. Image Process. **16** (2007), no. 3, 698–709.
25. AEO505D08F Specification Sheet, available at https://www.thorlabs.com/drawings/55097cd194019eb-FC53358D-C170-7584-85406F5F3CE937E2/AE0505D08F-SpecSheet.pdf
26. M. Paturzo et al., *Digital holography, a metrological tool for quantitative analysis: Trends and future applications*, Opt. Lasers Eng. **104** (2018), 32–47.
27. V. Pagliarulo et al., *Leaks detection in stainless steel kegs via ESPI*, Opt. Lasers Eng. **110** (2018), 220–227.
28. M. P. Georges et al., *An overview of interferometric metrology and NDT techniques and applications for the aerospace industry*, Proc. of SPIE **9960** (2016), Article no. 996007.
29. V. Antonucci et al., *Low velocity impact response of carbon fiber laminates fabricated by pulsed infusion: A review of damage investigation and semi-empirical models validation*, J. Progress Aerospace Sci. **81** (2016), 26–40.
30. V. Pagliarulo et al., *Combining ESPI with laser scanning for 3D characterization of racing tyres sections*, Opt. Lasers Eng. **104** (2018), 71–77.

AUTHOR BIOGRAPHIES

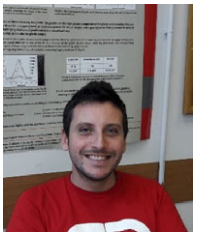

Vittorio Bianco received his MS degree (cum laude) in Telecommunications Engineering from the University of Naples Federico II in Naples, Italy. In 2016, he received his PhD degree in Materials and Structures Engineering. He won the IEEE Best Doctoral Thesis in Optoelectronics Award in 2016, assigned by the Italian chapter of the IEEE Photonics Society. In 2011, he worked at the German Aerospace Centre in Munich, Germany, in the fields of SAR interferometry, tomography, and SAR data processing. In 2017, he was a postdoctoral student in the Electrical Engineering Department of the University of California, Los Angeles (UCLA), USA, working in the field of lensless inline digital holography for biomedical imaging and point-of-care diagnostics. Since 2012, he has worked at the Italian National Research Council in the field of digital holography. His research activities include the fields of optics and image processing, computational microscopy, optical systems engineering, and image enhancement applied to microfluidics and diagnostics. He has authored more than 80 works in his fields of expertise.

Melania Paturzo received her MS degree (cum laude) in physics from the University of Naples Federico II, Naples, Italy, in 2002, and her PhD degree from the European Laboratory for Nonlinear Spectroscopy, University of Florence, Florence, Italy. She won the Best Doctoral Thesis Award from the Italian chapter of the Photonics Society of the Institute of Electrical and Electronic Engineers. She is currently a research scientist at the Institute of Applied Science and Intelligent Systems of the National Research Council, Pozzuoli, Naples, Italy. Her research interest includes the fields of optics and photonics. Her research activities concern the investigation of material properties by means of interferometric techniques, development of optical techniques to achieve super-resolution in digital holographic microscopy, holographic display, quantitative phase-contrast microscopy for cellular investigation, and optofluidics. She is an author and/or co-author of more than 130 papers in international peer-reviewed journals and of more than 90 conference papers (h-index 30).

Andrea Finizio has worked in the Optical Department of the Cybernetics Institute of the National Research Council of Naples, Italy, since 1968, managing the experimental activities of the optical laboratories. He has broad professional experience in the design of systems and laboratory techniques for display holography, conventional and digital holographic interferometry, and applications to nondestructive testing and optical metrology.

Pietro Ferraro graduated in physics, cum laude, from the University of Naples Federico II, Italy, in 1987. In 1993, he joined the optical group of the National Research Council at the Institute of Cybernetics of Pozzuoli, Naples, as an associate researcher to develop interferometric and holographic methods for testing and characterizing optical components and materials. Since 2005, he has been the head of a research group in optical diagnostics, interferometry, and microscopy. He is also the director of the Institute of Applied Sciences and Intelligent Systems. His research areas include laser interferometry, holography, holographic lithography, and the microstructure of ferroelectric crystals for photonic applications. He has published over 220 articles in peer-reviewed journals and over 200 conference papers. He was an editor of two books with Springer: *Micro-nano-engineering and characterization of ferroelectric crystals for photonic applications* and *Coherent light microscopy—Imaging and quantitative phase analysis*. He holds 12 patents. He was elected Fellow of the Optical Society of America in 2010 and Senior Member of the Institute of Electrical and Electronic Engineers in 2007.